



## Article

# Research and Application of the Original Position Statistical Distribution Analysis Method for Non-Metallic Inclusions in P91 Steel

Changwang Zhu <sup>1</sup>, Lixia Yang <sup>2,3,\*</sup> , Lei Zhao <sup>2,3</sup>, Yue Ma <sup>3</sup>, Yang Wang <sup>2,3</sup>, Xuejing Shen <sup>2,3</sup>  
and Haizhou Wang <sup>1,2,3,\*</sup> 

- <sup>1</sup> Beijing Advanced Innovation Center for Materials Genome Engineering, National Center for Materials Service Safety, University of Science and Technology Beijing, Beijing 100083, China  
<sup>2</sup> Beijing Advanced Innovation Center for Materials Genome Engineering, Central Iron & Steel Research Institute, Beijing 100081, China  
<sup>3</sup> Beijing Key Laboratory of Metal Materials Characterization, NCS Testing Technology Co., Ltd., Beijing 100081, China  
\* Correspondence: yanglixia@ncschina.com (L.Y.); wanghaizhou@ncschina.com (H.W.)

**Abstract:** Heat-resistant P91 martensitic steel is used to produce high-temperature steam pipelines in (ultra) critical power plants. However, non-metallic inclusions are inevitably produced in the metallurgical process. The type, composition, morphology, quantities, size and distribution of these inclusions have significant influences on the properties of materials. The present work developed an original position statistical distribution analysis method to characterize non-metallic inclusions in P91 steel based on scanning electron microscopy (SEM) with energy-dispersive spectroscopy (EDS). Two samples from P91 steel pipes fabricated by different processes were examined. The non-metallic inclusions in these samples could be divided into spherical oxides, strand-shaped oxides, spherical sulfides, spherical oxygen–sulfur compounds, strip sulfides and other inclusions. The amount, proportional area, particle sizes, original positions and statistical distribution results of non-metallic inclusions in different processed samples were assessed, and the causes and effects of these inclusions were analyzed. This novel method could provide diversified information on inclusions, which is helpful for the improvement of metallurgical processes and service performance evaluations.

**Keywords:** martensitic heat-resistant P91 steel; non-metallic inclusions; scanning electron microscopy (SEM); original position statistical distribution analysis method



**Citation:** Zhu, C.; Yang, L.; Zhao, L.; Ma, Y.; Wang, Y.; Shen, X.; Wang, H. Research and Application of the Original Position Statistical Distribution Analysis Method for Non-Metallic Inclusions in P91 Steel. *Metals* **2023**, *13*, 793. <https://doi.org/10.3390/met13040793>

Academic Editor: Mark E. Schlesinger

Received: 9 March 2023

Revised: 6 April 2023

Accepted: 13 April 2023

Published: 17 April 2023



**Copyright:** © 2023 by the authors. Licensee MDPI, Basel, Switzerland. This article is an open access article distributed under the terms and conditions of the Creative Commons Attribution (CC BY) license (<https://creativecommons.org/licenses/by/4.0/>).

## 1. Introduction

Heat-resistant P91 martensitic steel has become the primary steel in thermal power plants constructed in China in the 21st century. It has good high-temperature strength, exceptional thermal conductivity, a low coefficient of thermal expansion, oxidation resistance and good processing performance [1–3]. Importantly, non-metallic inclusions in steel can significantly affect the characteristics of materials. In particular, large inclusions can seriously deteriorate the fatigue performance of steel [4]. Non-metallic inclusions can also appear as undesirable second-phase particles in linepipe steels, and they may have a significant effect on the mechanical properties and surface qualities of these materials [5]. Inclusions in steel are generally non-metallic particles produced or mixed in during smelting and pouring processes. These can comprise compounds formed by the reaction of certain metallic elements (including iron, manganese, aluminum, etc.) with non-metallic elements (e.g., oxygen, sulfur, nitrogen, phosphorus and carbon), and they consist primarily of oxides and sulfides [6]. P91 steel is typically deoxidized by adding aluminum during the smelting process such that many Al<sub>2</sub>O<sub>3</sub> inclusions possessing high melting points and other types of inclusions can be produced during deoxidation process.

The  $\text{Al}_2\text{O}_3$  inclusions with high melting points can cause nozzle plugging or degrade the surface quality of steel pipes [7]. The inclusion type, composition, shape, quantity, size and other state properties of non-metallic inclusions can all affect the properties of steel [8].

Currently, optical microscopy, scanning electron microscopy (SEM) with energy-dispersive spectroscopy (EDS) and analyses based on atomic emission spectroscopy are all introduced to study inclusions on the surfaces of metallic materials. Optical microscopy allows the morphological characteristics of inclusions to be examined, but it is challenged to detect inclusions in larger samples. It is also difficult to obtain other information such as the quantity of inclusions quickly and accurately [9,10]. SEM is commonly used to characterize non-metallic inclusions and can assess the size, type and quantity of inclusions. However, there has been little research concerning the information related to the location of inclusions [11,12]. Li et al. [13] ascertained the size distribution of inclusions using a spark discharge atomic emission spectrometer. This process can rapidly analyze large samples but cannot accurately identify small inclusions. Wang et al. [14] analyzed the composition and size of aluminum inclusions in medium and low alloy steel using laser-induced breakdown spectroscopy (LIBS). The sample preparation required for this methodology is simple, and the analysis is rapid, but the actual morphologies of inclusions cannot be determined. The GB/T 30834-2014 standard for the statistical assessment of non-metallic inclusions in steel by SEM classifies non-metallic inclusions in P91 steel as type A, C, D or DS. However, P91 steel contains spherical oxides, spherical sulfides, strip sulfides, strand oxides, spherical oxygen–sulfur compounds, titanium-bearing and other inclusions [15]. The method outlined in this standard allows the quantity, area and size of non-metallic inclusions in P91 to be evaluated still, it does not provide a statistical distribution analysis of original location information or permit other quantitative parameters to be investigated.

The present work develops an original position statistical distribution analysis method for characterizing non-metallic inclusions in P91 steel based on SEM combined with EDS. Using this technique, the quantity, area and size distribution of non-metallic inclusions in steel are ascertained, and the original location information of these non-metallic inclusions is also analyzed. The composition of these inclusions and the associated formation mechanisms are discussed.

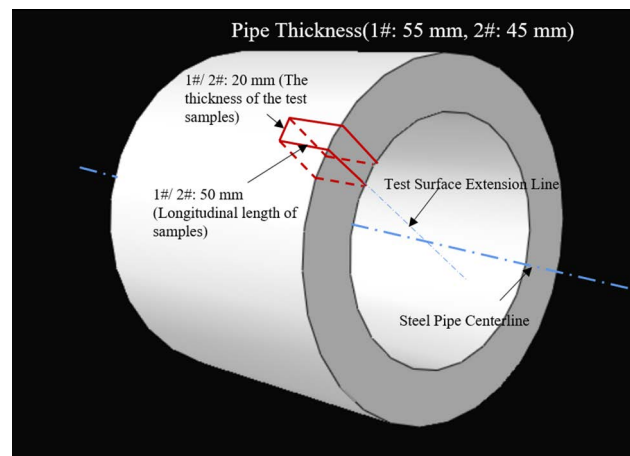
## 2. Materials and Methods

The P91 specimens, referred to herein as sample 1# and sample 2#, were excised from steel pipes with wall thicknesses of 55 and 45 mm, respectively. These steel samples had been subjected to a series of processes comprising electric furnace smelting, ladle furnace heating, vacuum treatment, die casting, forging, annealing, pipe rolling and heat treatment. In addition, different controls were applied to the content of S in the steels. The composition of both materials is summarized in Table 1.

**Table 1.** Main elemental composition of P91 steel pipe samples (wt.%).

| Samples No. | C    | Si   | Mn   | P     | S      | Cr   | Ni   | Cu    | Mo   | V    | Nb    | Al     | Ti     | N     | O      | Fe   |
|-------------|------|------|------|-------|--------|------|------|-------|------|------|-------|--------|--------|-------|--------|------|
| 1#          | 0.11 | 0.28 | 0.42 | 0.012 | 0.0024 | 8.72 | 0.14 | 0.035 | 0.91 | 0.20 | 0.078 | <0.005 | <0.001 | 0.048 | 0.0018 | Bal. |
| 2#          | 0.12 | 0.30 | 0.37 | 0.011 | 0.0010 | 8.67 | 0.16 | 0.031 | 0.93 | 0.20 | 0.074 | <0.005 | <0.001 | 0.044 | 0.0022 | Bal. |

Both samples were cut along the longitudinal section of the steel pipes. Sample 1# and sample 2# had dimensions of  $55 \times 50 \times 20$  mm and  $45 \times 50 \times 20$  mm, respectively, as shown in Figure 1. Based on standard metallographic sample preparation methods, the samples were subjected to rough grinding, fine grinding, polishing and then cleaned with absolute ethanol and dried. A longitudinal section of each sample passing through the centerline was analyzed to explore the distribution of inclusions from the inner wall to the outer wall of the pipe. The analyzed areas of samples 1# and 2# were 365 and 333 mm<sup>2</sup>, respectively.



**Figure 1.** A diagram showing the sampling location from the steel pipes were sampled.

A tungsten filament SEM instrument (TESCAN VEGA3, Tescan Corp., Brno, Czech Republic) combined with energy spectrum analysis software (Aztec, Oxford Instruments Corp., Oxford, UK) was used for particle detection and analysis. The selection of various SEM parameters is known to affect the accuracy of particle detection and the quality of the images that are obtained. Based on the typical morphology of non-metallic inclusions in P91 steel, an acceleration voltage of 20 kV and beam current of 15  $\mu$ A were selected. A working distance of 10 mm was employed to ensure good image quality. Using a magnification of 300 $\times$  and image resolution of 2048, the minimum size of inclusions that could be detected was 0.38  $\mu$ m. An acquisition time of 0.5 s was used, providing a high identification accuracy of 0.9  $\mu$ m and allowing the inclusions to be counted. Aluminum foil was pasted to one edge of each sample to calibrate the grayscale of the images such that the brightness value of the aluminum foil was 5120 and that of the steel was 25,700. The SEM system automatically identified any zone with a brightness of less than 23,000 as an inclusion [16,17]. The test parameters are shown in Table 2.

**Table 2.** Instrument parameters.

| Instrument Parameters                 | Numerical Value    |
|---------------------------------------|--------------------|
| Electron microscope high voltage (kV) | 20                 |
| First pass residence time ( $\mu$ s)  | 5                  |
| Analysis mode                         | Particle detection |
| Energy range (keV)                    | 40                 |
| Number of channels                    | 1024               |
| Acquisition time (s)                  | 0.50               |
| Image scan size                       | 2048               |
| Image magnification                   | 300                |
| Image pixel resolution ( $\mu$ m)     | 0.90               |
| Working distance (mm)                 | 10                 |
| Beam intensity ( $\mu$ A)             | 15                 |

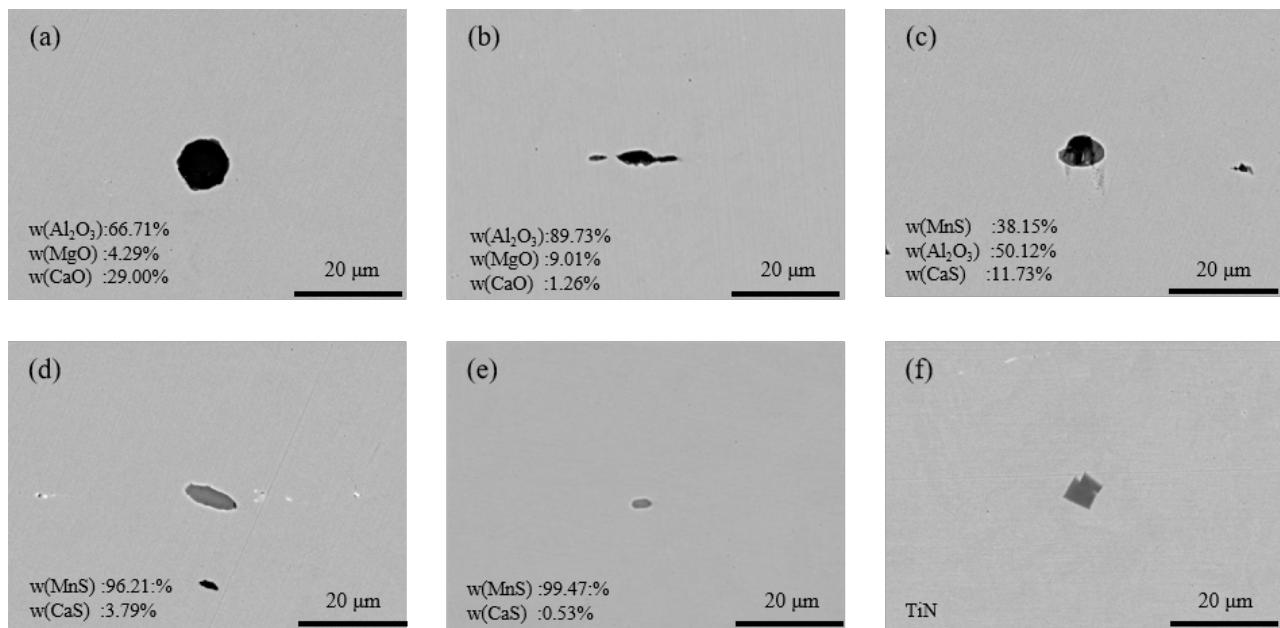
Data concerning inclusions in the P91 steel pipes along the longitudinal direction from the inner to the outer wall were collected using SEM together with the particle detection and analysis module of the energy spectrometer. The compositions and morphologies data of inclusions were analyzed, and the inclusions were classified and counted.

### 3. Results and Discussion

#### 3.1. Classification of Non-Metallic Inclusions

The main types of non-metallic inclusions and the typical characteristics of non-metallic inclusions in P91 steel samples are summarized in Figure 2 and Table 3. Figure 2a

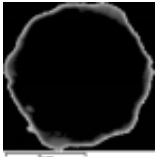

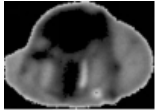


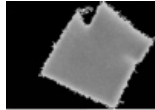
and Table 3 (column (a)) show an  $\text{Al}_2\text{O}_3$ -MgO-CaO inclusion with an aspect ratio of less than 3 and a roughly spherical shape. This inclusion appeared black in the back-scattered electron image and contained 66.71%  $\text{Al}_2\text{O}_3$ , 4.29% MgO and 29.00% CaO. These inclusions were therefore primarily made of  $\text{Al}_2\text{O}_3$  along with a small number of (Al, Mg, Ca and Si) O inclusions in which the Si content was less than the others. Figure 2b and Table 3 (column (b)) show an  $\text{Al}_2\text{O}_3$ -MgO-CaO inclusion in the form of a long strand with an aspect ratio greater than 3. This inclusion also appeared black and contained 89.73% of  $\text{Al}_2\text{O}_3$ , 9.01% of MgO and 1.26% of CaO along with a small amount of S element. The spherical inclusion in Figure 2c and Table 3 (column (c)) was an  $\text{Al}_2\text{O}_3$ -MnS-CaS composite with an aspect ratio of less than 3. The oxide part of the BSE image was black while the sulfide part was gray. This inclusion comprised 38.15% of  $\text{Al}_2\text{O}_3$ , 50.12% of MnS and 11.73% of CaS. The energy spectrum indicated that this inclusion was made of 16.9% S, 23.1% Al and 31.6% O on a mass basis. Figure 2d and Table 3 (column (d)) presented a BSE image of a gray MnS-CaS inclusion with an aspect ratio greater than 3 and containing 96.21% MnS and 3.79% CaS. The gray, spherical MnS-CaS inclusion in Figure 2e and Table 3 (column (e)) had an aspect ratio of less than 3 and contained 99.47% MnS and 0.53% CaS. Figure 2f and Table 3 (column (f)) show a gray TiN inclusion with an aspect ratio of less than 3 along with a small amount of elemental Nb and V.



**Figure 2.** A summary of the types of non-metallic inclusions. (a) Spherical  $\text{Al}_2\text{O}_3$ -MgO-CaO, (b) a long strand of  $\text{Al}_2\text{O}_3$ -MgO-CaO, (c) an  $\text{Al}_2\text{O}_3$ -MnS-CaS composite, (d) a MnS-CaS strand, (e) spherical MnS-CaS, and (f) titanium-bearing inclusions.

These data indicated that the inclusions were mainly made of aluminum oxides, unfortunately, only a qualitative compositional analysis was possible because oxygen had a low atomic number with a low energy spectrum signal. However, the presence of aluminum and sulfur in the energy spectrum could be used to identify and classify these inclusions. Therefore, based on both chemical composition and morphologies, the inclusions were classified according to the rules presented in Table 4.

**Table 3.** Characteristics of typical non-metallic inclusions.

| Inclusion Characteristics   | (a)                                                                               | (b)                                                                               | (c)                                                                               | (d)                                                                                | (e)                                                                                 | (f)                                                                                 |
|-----------------------------|-----------------------------------------------------------------------------------|-----------------------------------------------------------------------------------|-----------------------------------------------------------------------------------|------------------------------------------------------------------------------------|-------------------------------------------------------------------------------------|-------------------------------------------------------------------------------------|
| Inclusion morphology        |  |  |  |  |  |  |
| Area( $\mu\text{m}^2$ )     | 12.52                                                                             | 12.93                                                                             | 26.16                                                                             | 24.61                                                                              | 4.44                                                                                | 28.90                                                                               |
| Length( $\mu\text{m}$ )     | 9.88                                                                              | 15.35                                                                             | 8.19                                                                              | 9.82                                                                               | 3.48                                                                                | 9.77                                                                                |
| Aspect ratio                | 1.09                                                                              | 4.76                                                                              | 1.43                                                                              | 3.03                                                                               | 2.15                                                                                | 1.59                                                                                |
| ECD( $\mu\text{m}$ )        | 3.99                                                                              | 4.06                                                                              | 5.77                                                                              | 16.28                                                                              | 2.38                                                                                | 6.07                                                                                |
| Chemical composition (wt.%) | O:50.8                                                                            | O:51.3                                                                            | O:31.6                                                                            | Al:0.4                                                                             | Mn:65.5                                                                             | Ti:54.4                                                                             |
|                             | Al:29.2                                                                           | Al:37.0                                                                           | Al:23.1                                                                           | Mn:56.3                                                                            | Ca:0.4                                                                              | N:31.7                                                                              |
|                             | Ca:17.1                                                                           | Ca:5.7                                                                            | Mn:21.0                                                                           | Ca:2.5                                                                             | S:34.1                                                                              | Nb:8.1                                                                              |
|                             | Mg:2.1                                                                            | Mg:0.7                                                                            | Ca:7.2                                                                            | S:40.7                                                                             |                                                                                     | V:5.8                                                                               |
|                             | S:0.8                                                                             | S:4.2                                                                             | S:16.9                                                                            |                                                                                    |                                                                                     |                                                                                     |

**Table 4.** The classification rules of inclusions.

| Number | Inclusion Type                                                                              | Identifying Elements   | Element Mass Percentage (wt.%) | Aspect Ratio           |
|--------|---------------------------------------------------------------------------------------------|------------------------|--------------------------------|------------------------|
| 1      | Spherical oxide ( $\text{Al}_2\text{O}_3$ )                                                 | Al/S                   | $0 \leq \text{S/Al} < 1$       | $1 \leq \text{AR} < 3$ |
| 2      | Strand oxide ( $\text{Al}_2\text{O}_3$ )                                                    | Al/S                   | $0 \leq \text{S/Al} < 1$       | $\text{AR} \geq 3$     |
| 3      | Spherical sulfide ( $\text{MnS}$ , $\text{CaS}$ )                                           | Al/S                   | $\text{S/Al} \geq 3$           | $1 \leq \text{AR} < 3$ |
| 4      | Strip sulfide ( $\text{MnS}$ , $\text{CaS}$ )                                               | Al/S                   | $\text{S/Al} \geq 3$           | $\text{AR} \geq 3$     |
| 5      | Spherical oxygen–sulfur compounds ( $\text{Al}_2\text{O}_3$ , $\text{MnS}$ , $\text{CaS}$ ) | Al/S                   | $1 \leq \text{S/Al} < 3$       | $1 \leq \text{AR} < 3$ |
| 6      | Titanium-bearing inclusions                                                                 | Ti, excluding Al and S | /                              | /                      |

### 3.2. Statistical Analysis

Using the classification rules outlined in Table 4, the non-metallic inclusions with equivalent circle diameter (ECD) values were greater than 1  $\mu\text{m}$  were categorized and counted using the particle detection module of the software associated with the SEM. ECD is the diameter of the circle with the same area as the inclusion. Table 5 summarizes the proportional quantities of various inclusions in both steel pipe specimens. The most common non-metallic inclusions were spherical oxides, spherical sulfides and spherical oxygen–sulfur compounds. Table 6 provided the proportional area occupied by various inclusions and indicated that the spherical oxides accounted for the largest area. This occurred because the spherical oxides were generally larger than the spherical sulfide and spherical oxygen–sulfur compounds. Only a small number of strip sulfides and oxide strands was observed, but the relative area occupied by these inclusions was quite large. In addition, the number of sulfide inclusions in sample 1# and the area occupied by these inclusions were both higher those in sample 2#. The amount and proportional area of titanium-bearing inclusions were very small, so these inclusions were neglected.

**Table 5.** The quantities of various inclusions found in 100  $\text{mm}^2$  sections of steel samples.

| Samples                    | Spherical Oxide | Strand Oxide | Striped Sulfide | Spherical Sulfide | Spherical Oxygen–Sulfur Compounds | Ti-Bearing Inclusions | Total |
|----------------------------|-----------------|--------------|-----------------|-------------------|-----------------------------------|-----------------------|-------|
| Proportion of Quantity (%) |                 |              |                 |                   |                                   |                       |       |
| 1#                         | 64.75           | 0.99         | 2.97            | 22.82             | 8.41                              | 0.06                  | 1     |
| 2#                         | 96.31           | 0.92         | 0.17            | 1.75              | 0.81                              | 0.04                  | 1     |

**Table 6.** The proportional area occupied by various inclusions in 100 mm<sup>2</sup> sections of steel samples.

| Samples             | Spherical Oxide | Strand Oxide | Striped Sulfide | Spherical Sulfide | Spherical Oxygen–Sulfur Compounds | Ti Inclusions | Total |
|---------------------|-----------------|--------------|-----------------|-------------------|-----------------------------------|---------------|-------|
| Area Proportion (%) |                 |              |                 |                   |                                   |               |       |
| 1#                  | 77.52           | 2.26         | 5.74            | 9.42              | 4.91                              | 0.15          | 1     |
| 2#                  | 91.29           | 6.61         | 0.41            | 1.10              | 0.58                              | 0.01          | 1     |

### 3.3. Size Distribution of Inclusions

Tables 7 and 8 provided the size distribution of the inclusions in the steel pipe samples. In the case of inclusions with aspect ratios less than 3, the ECD was used as the size for statistical analysis purposes. For inclusions with aspect ratios greater than 3, the maximum length was employed.

**Table 7.** Results of the particle size distribution of inclusions in 100 mm<sup>2</sup> of Sample 1#.

| Particle Size/ $\mu\text{m}$ | Spherical Oxide | Strand Oxide | Striped Sulfide | Spherical Sulfide | Spherical Oxygen–Sulfur Compounds |
|------------------------------|-----------------|--------------|-----------------|-------------------|-----------------------------------|
| Quantity                     |                 |              |                 |                   |                                   |
| 1~3                          | 166             | 1            | 2               | 163               | 38                                |
| 3~5                          | 264             | 0            | 0               | 49                | 38                                |
| 5~7                          | 139             | 0            | 1               | 7                 | 5                                 |
| 7~10                         | 48              | 2            | 8               | 2                 | 1                                 |
| 10~13                        | 6               | 2            | 7               | 0                 | 0                                 |
| >13                          | 3               | 4            | 10              | 0                 | 0                                 |
| Total                        | 627             | 9            | 28              | 221               | 82                                |
| Maximum ECD/ $\mu\text{m}$   | 27.0            | 28.9         | 35.9            | 14.5              | 7.1                               |

**Table 8.** Results of the particle size distribution of inclusions in 100 mm<sup>2</sup> of Sample 2#.

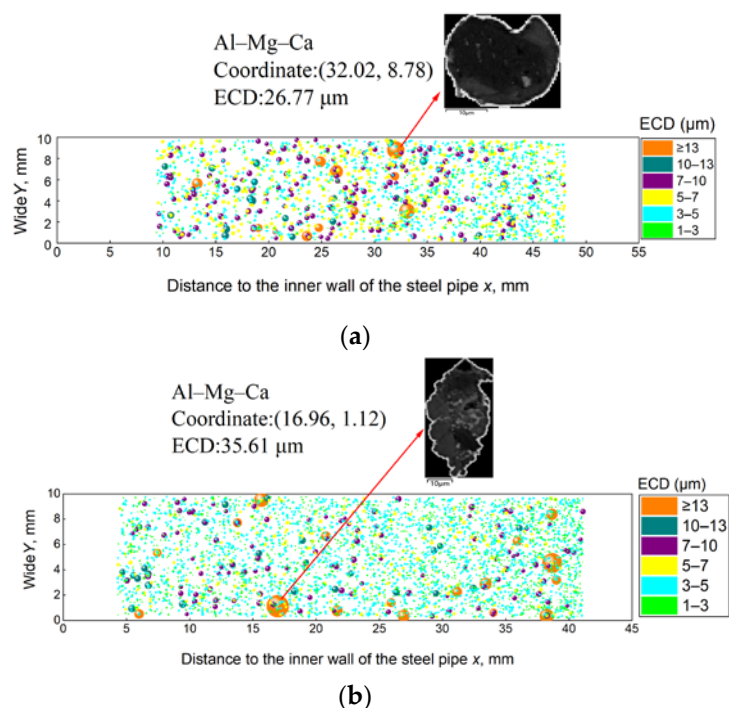
| Particle Size/ $\mu\text{m}$ | Spherical Oxide | Strand Oxide | Striped Sulfide | Spherical Sulfide | Spherical Oxygen–Sulfur Compounds |
|------------------------------|-----------------|--------------|-----------------|-------------------|-----------------------------------|
| Quantity (%)                 |                 |              |                 |                   |                                   |
| 1~3                          | 615             | 0            | 1               | 19                | 9                                 |
| 3~5                          | 639             | 0            | 0               | 4                 | 2                                 |
| 5~7                          | 88              | 0            | 0               | 2                 | 0                                 |
| 7~10                         | 34              | 2            | 0               | 1                 | 0                                 |
| 10~13                        | 8               | 3            | 1               | 0                 | 0                                 |
| >13                          | 5               | 8            | 1               | 0                 | 0                                 |
| Total                        | 1389            | 13           | 2               | 25                | 12                                |
| Maximum ECD/ $\mu\text{m}$   | 35.6            | 43.9         | 18.1            | 8.8               | 10.6                              |

It can be observed from Table 7 that the spherical oxides had sizes concentrated within the range of 1–7  $\mu\text{m}$ , but three larger oxide particles were observed, and the maximum ECD was 27.0  $\mu\text{m}$ . There were far fewer strand oxide and strip sulfide inclusions, but these had relatively large lengths. The spherical sulfide and spherical oxygen–sulfur compounds were small and had sizes primarily within 1–5  $\mu\text{m}$ . After the ECD distribution of spherical sulfide inclusions was converted into a size distribution based on the unit area, no large inclusions were identified although an inclusion with an ECD of 14.5  $\mu\text{m}$  was observed in the test area. There were two titanium-bearing inclusions in the region that was inspected, with sizes of 9.34 and 4.22  $\mu\text{m}$ . The data for sample 2# in Table 8 show that the spherical oxide inclusions had sizes within the range of 1–7  $\mu\text{m}$ , and there were close to twice as many of these inclusions in this sample as there were in sample 1#. One spherical oxide inclusion

had a maximum ECD of 35.6  $\mu\text{m}$ . There were few strand oxide inclusions, although one large inclusion with a size of 43.9  $\mu\text{m}$  was found. There were many strip sulfide, spherical sulfide and oxygen–sulfur composite inclusions in sample 1#, including 10 strip sulfides larger than 13  $\mu\text{m}$ , while sample 2# contained mainly spherical oxides.

### 3.4. Original Statistical Distribution Analysis of Spherical Oxides

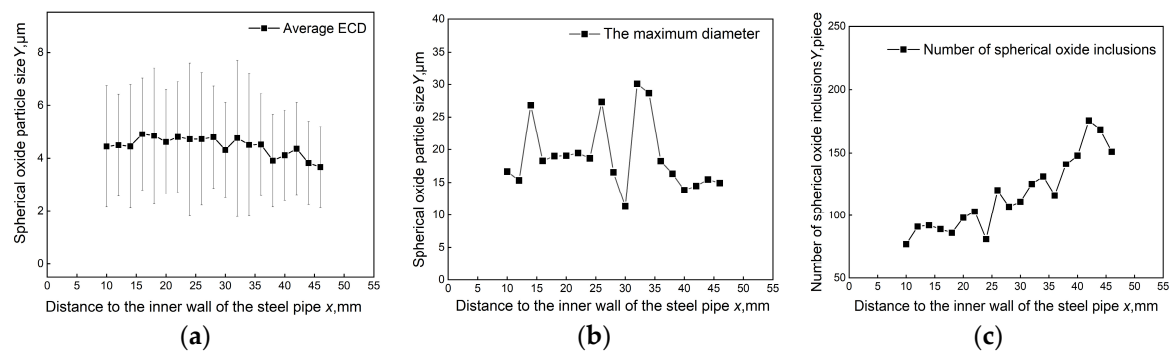
As noted, the present steel specimens contained numerous spherical oxide inclusions, and the size distribution and location of these inclusions were therefore important with regard to metallurgical processing and the evaluation of such materials. Figure 3a,b presented images showing the original statistical distribution of the spherical oxides based on ECD proceeding from the inner to outer wall of the steel pipes. To allow the sizes and distribution of the inclusions to be accurately assessed, the inclusions were magnified by a factor of 50, and the largest spherical oxide in the test area was indicated (The inclusion indicated by the red arrow in the Figure 3a,b). In the case of sample 1#, the spherical oxide inclusions near the outer part of the steel pipe were smaller than those in the inner part, although larger inclusions were also presented in the middle. The largest inclusion size was 26.77  $\mu\text{m}$  in size and contained Al, Mg and Ca. There was no obvious trend in the distribution of inclusions in sample 2#. This specimen contained an oxide inclusion made of Al, Mg and Ca with a size of 35.61  $\mu\text{m}$ .



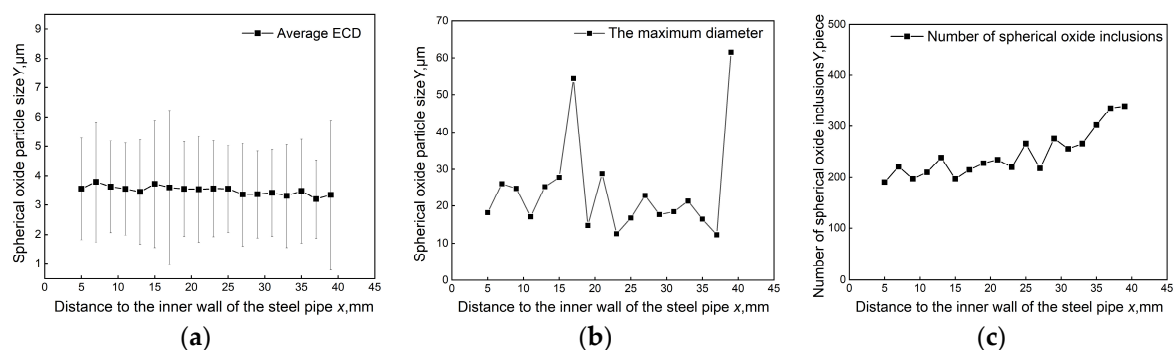
**Figure 3.** Original statistical distribution of non-metallic spherical oxide inclusions based on ECD in (a) sample 1# and (b) sample 2#.

During the solidification of liquid steel, the cooling rate at the outer wall was more rapid such that dendrites formed, and larger inclusions were pushed to the central area. Subsequent pipe threading and rolling processes could also break up large inclusions on the inner wall, explaining why the larger inclusions were found in the central region. These effects also generated many inclusions along the inner wall of the steel pipe. The negative effect of larger inclusions was greater, so this work focused on these inclusions. Figures 4 and 5 plot the ECD values, maximum sizes and quantities of spherical oxide inclusions proceeding from the inside of the steel pipe to the outside for samples 1# and 2#, respectively. The spherical oxide ECD values for sample 1# exhibited a decreasing trend when proceeding from the inner wall to the outer wall, as did the maximum diameters.

However, the data also showed significant fluctuations in the middle area and the presence of some large inclusions. The number of inclusions increased when proceeding from the inner wall to the outer wall, with an increase from 77 to 175. The data for sample 2# demonstrated similar trends, with the quantity of inclusions increasing from 190 to 339. Compared with those in sample 1#, the average ECD values in sample 2# were both smaller and more uniform. However, the trend of the number of inner and outer walls changed substantially.



**Figure 4.** Average ECD values in graphic (a), maximum size in graphic (b) and quantity of spherical oxide inclusions in graphic (c) along the cross-section of sample 1#.



**Figure 5.** Average ECD values in graphic (a), maximum size in graphic (b) and quantity of spherical oxide inclusions in graphic (c) along the cross-section of sample 2#.

### 3.5. Formation Mechanism and the Effect of the Inclusions

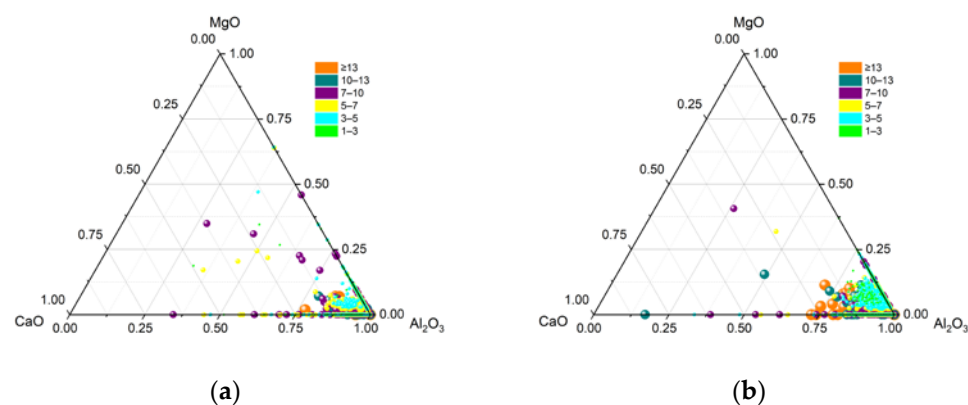
From the above experimental results, it can be observed that the sizes of various inclusions in the steel pipes are small. The data in Tables 9 and 10 indicate that the majority most inclusions contained Al, followed by those containing Ca and Mg. Sample 1# contained more CaO, while there was more MgO in sample 2#. The oxide compositions and size distribution in the steel pipes are summarized in Figure 6. These graphs are based on the analysis of 2019 inclusions for sample 1# and 4626 inclusions for sample 2#. It was apparent that MgO-Al<sub>2</sub>O<sub>3</sub>, CaO-Al<sub>2</sub>O<sub>3</sub> and CaO-Al<sub>2</sub>O<sub>3</sub>-MgO were the main inclusions with a high melting point in these steel specimens and that the primary component of the inclusions was alumina. Those inclusions with high calcium oxide concentrations were also relatively large, and sample 1# contained more of these inclusions. Overall, sample 1# contained oxide inclusions with greater average ECD values.

**Table 9.** Quantities of inclusions with different compositions within a 100 mm<sup>2</sup> region of sample 1#.

| Inclusions Type       | Quantity/Unit | Percentage/% |
|-----------------------|---------------|--------------|
| Al-bearing inclusions | 2855          | 80.8         |
| Mg-bearing inclusions | 869           | 24.6         |
| Si-bearing inclusions | 184           | 5.2          |
| Ca-bearing inclusions | 1301          | 36.8         |

**Table 10.** Quantities of inclusions with different compositions within 100 mm<sup>2</sup> region of sample 2#.

| Inclusions Type       | Quantity/Unit | Percentage/% |
|-----------------------|---------------|--------------|
| Al-bearing inclusions | 4722          | 98.3         |
| Mg-bearing inclusions | 2182          | 45.4         |
| Si-bearing inclusions | 195           | 4.1          |
| Ca-bearing inclusions | 1175          | 24.5         |

**Figure 6.** Composition and size distribution. Phase diagrams for inclusions in (a) Sample 1# and (b) Sample 2#.

The total oxygen content of the steel pipe had a significant effect on the number and size of oxide inclusions. Yu [18] reported that the amount and area of inclusions in a steel pipe containing 0.01% oxygen increased compared to steel with 0.002% oxygen. He [19] demonstrated that the quantity of 5–10  $\mu\text{m}$  inclusions decreased as the total oxygen content decreased. In the present study, the oxygen concentrations of the pipe specimens were 0.0018% and 0.0022%, and the majority of spherical oxides had sizes within the range of 3–5  $\mu\text{m}$ . In addition, even the largest such inclusions were not overly large. The primary inclusions in these steel pipes were spherical oxides that consisted largely of alumina and these results are believed to be related to the Al alloy deoxygenation process. Inclusions in melted steel are generated via the sequence  $\text{Al}_2\text{O}_3 \rightarrow \text{MgO-Al}_2\text{O}_3 \rightarrow \text{CaO-Al}_2\text{O}_3\text{-MgO}$  or  $\text{CaO-Al}_2\text{O}_3$  [20,21]. The strand-shaped oxide inclusions that were observed could have resulted from a lack of floating following deoxidation combined with breaking into long chains during rolling [22]. Al-bearing oxides in steel are also formed as a consequence of the secondary oxidation [23] of refractories and molten steel. Currently, the main method used to modify inclusions in steel subjected to aluminum deoxygenation involves treatment with calcium. In this process,  $\text{Al}_2\text{O}_3$  and  $\text{Al}_2\text{O}_3\text{-MgO}$  inclusions are modified to form calcium aluminate inclusions with low melting points. This reduces the effects of  $\text{Al}_2\text{O}_3$  and magnesium aluminum spinel on the performance characteristics of the metal [24,25].

Murakami et al. [26] devised an empirical relationship between the fatigue limit of steel and Vickers hardness and inclusion size applicable to different fatigue test conditions. Based on this relationship, Li et al. [27] calculated the critical inclusion size for pipeline steel to reach the fatigue limit. Li reported that large inclusions located below the metal surface could have a relatively pronounced impact on fatigue performance, while large internal inclusions have a minimal effect. However, a few large type- D inclusions were

found in the present experimental samples and were located primarily in the interior of samples such that these inclusions would be expected to have little effect on the steel.

As early as the 1980s, Ito et al., classified sulfides in low-carbon steel into Class I spherical sulfides, Class II fan-shaped or chain sulfides, Class III polyhedral sulfides and irregular sulfides [28]. The morphology of inclusions varies with sulfur content [29]. In the present study, sulfide inclusions were primarily found in sample 1#, which had a sulfur content of 0.0024%. Spherical sulfide inclusions accounted for 24% of all inclusions and were mainly made of MnS. After the size distribution of spherical sulfide inclusions was converted into a size distribution per unit area, an inclusion with an ECD of 14.5  $\mu\text{m}$  was identified along with 29 strip-shaped sulfides occupying a large area. The amount of spherical sulfide inclusions in the P91 steel was low, and the sulfide size of composite CaS was small, while the percentage of CaS in strip-shaped sulfides was less than that in spherical sulfide inclusions. The addition of calcium and magnesium as alloying elements, especially calcium, will significantly reduce the length-to-width ratio and size of sulfide inclusions [30]. The present oxygen–sulfur composite inclusions were MnS–Al<sub>2</sub>O<sub>3</sub> inclusions formed by fine oxide particles acting as cores for heterogeneous nucleation. The formation of these inclusions in steel inhibits the effects of oxides on the characteristics of the metal and can effectively prevent the initiation and propagation of cracks starting with oxides. The oxygen–sulfur composite inclusions identified in this study were relatively small, and none had an ECD greater than 13 microns. The titanium-bearing inclusions comprised titanium nitride, titanium carbide, titanium carbonitride and titanium oxide. There was also evidently competition between the oxidation reactions of aluminum and titanium. The Ti content of the steel was less than 0.001%, and the two samples all went through process of aluminum deoxidization. The sample had very few titanium-bearing inclusions [31–33].

#### 4. Conclusions

A statistical characterization method was developed that allowed an evaluation of non-metallic inclusions in P91 steel pipes based on SEM. The quantities, area and sizes of spherical oxide, strand oxide, spherical sulfide, oxygen–sulfur composite, strip sulfide and titanium-bearing inclusions were analyzed. In addition, the original position statistical distribution of spherical oxide inclusions was investigated, and inclusion locations were assessed.

The P91 steel contained primarily spherical oxide inclusions and fewer sulfide inclusions with smaller sizes. However, this material also had a small number of large inclusions located in the middle of the pipe that would be expected to have a bad impact on the performance of the steel. In addition, the oxide inclusions were not only mainly made of alumina but also contained Mg and Ca. These inclusions would likely reduce the effect of spinel inclusions on the performance characteristics of the steel. Furthermore, this method is believed to have significant promise with regard to the statistical analysis of non-metallic inclusions during the smelting and production of P91 steel.

**Author Contributions:** Conceptualization, C.Z. and L.Y.; data curation, C.Z.; formal analysis, L.Y.; funding acquisition, X.S.; investigation, C.Z.; methodology, C.Z.; project administration, L.Y.; resources, X.S.; software, L.Y.; supervision, H.W.; validation, L.Z., Y.M., Y.W. and H.W.; visualization, C.Z.; writing—original draft, C.Z.; writing—review and editing, L.Y. and H.W. All authors have read and agreed to the published version of the manuscript.

**Funding:** This work was financially supported by the National Key Research and Development Program of China (No. 2022YFB3707100) and the National Natural Science Foundation of China (No. 52075509).

**Data Availability Statement:** Research data are available upon reasonable request to the authors.

**Conflicts of Interest:** The authors declare no conflict of interest.

## References

- Guo, Y.; Wu, H. Research progress on localization of P91 seamless steel pipe. *Steel Pipes* **2008**, *39*, 22–27.
- Weng, L.; Chen, F.; Zhang, Y.; Xue, H.; De, L. Analysis of microstructure and mechanical properties of T/P91 high temperature furnace tube after service. *Hot Work. Technol.* **2020**, *49*, 133–135.
- Kim, W.; Lee, H.; Hong, H. Evaluation of tension and creep rupture behaviors of long-term exposed P91 steel in a supercritical plant. *Eng. Fail. Anal.* **2020**, *116*, 104736. [[CrossRef](#)]
- Yu, S.; Yang, K.; Lei, Y.; Yang, H. Grain refinement in heat affected zone of high strength low alloy steel welded with high heat input. *Trans. Chin. Weld. Institute* **2008**, *17–20*, 153–154.
- Chu, Y.; Li, W.; Ren, Y.; Zhang, L. Transformation of inclusions in linepipe steels during heat treatment. *Metall. Mater. Trans. B* **2019**, *50*, 2047–2062. [[CrossRef](#)]
- Zhang, Y.; Wu, J.; Miu, L. Analysis and research progress of non-metallic inclusions in steel. *Baosteel. Technol.* **2008**, *02*, 35–40.
- Lyu, S.; Ma, X.; Huang, Z.; YAO, Z.; Lee, H.; Jiang, Z.; Wang, G.; Zou, J.; Zhao, B. Inclusion characterization and formation mechanisms in spring steel deoxidized by silicon. *Metall. Mater. Trans. B* **2019**, *50*, 732–747. [[CrossRef](#)]
- Zhang, S.; Wang, H.; Wang, C. Discussion on classification method of non-metallic inclusions measured by scanning electron microscope. *Metal. Anal.* **2020**, *40*, 7–16.
- Wang, Z.; Xing, Z.; Wang, H.; Shan, X. Research progress on the effect of non-metallic inclusion characteristics on fatigue properties of iron and steel materials. *J. Mater. Eng.* **2020**, *48*, 1–12.
- Zhitenev, A.; Salynova, M.; Shamshurin, A.; Ryaboshuk, S.; Kolnyshenko, V. Database Clustering after Automatic Feature Analysis of Nonmetallic Inclusions in Steel. *Metals* **2021**, *11*, 1650. [[CrossRef](#)]
- Yuan, X.; Zhong, M.; Wu, Y.; Wang, C. Characterizing Inclusions in the Weld Metal of EH36 Shipbuilding Steel Processed by CaF<sub>2</sub>-30 Wt Pct TiO<sub>2</sub> Flux. *Metall. Mater. Trans. B* **2022**, *53*, 656–661. [[CrossRef](#)]
- Nabeel, M.; Alba, M.; Karasev, A.; Jönsson, P.; Dogan, N. Characterization of inclusions in 3rd generation advanced high-strength steels. *Metall. Mater. Trans. B* **2019**, *50*, 1674–1685. [[CrossRef](#)]
- LI, D.; SI, H.; Li, M.; Jia, Y.; Wang, H. In situ statistical distribution analysis of silicon inclusions in steel. *Metal. Anal.* **2009**, *29*, 1–7.
- Wang, H.; Jia, Y.; Li, Y.; Zhao, L.; Yang, C.; Cheng, D. Rapid analysis of content and particle sizes of aluminum inclusions in low and middle alloy steel by laser-induced breakdown spectroscopy. *Spectrochimica. Acta. B* **2020**, *171*, 105927. [[CrossRef](#)]
- ASTM E2412-08; Standard Test Methods for Rating and Classifying Inclusions in Steel Using the Scanning Electron Microscope. ASTM: West Conshohocken, PA, USA, 2015; 14p.
- Yan, C.; Yin, L.; Ren, Q.; Meng, Y.; Qi, Q. Discussion on influencing factors of SEM automatic statistical analysis results of inclusions in steel. *Metall. Anal.* **2018**, *38*, 1–10.
- Peng, Y.; Li, D.; Zhou, Q.; Zhao, L.; Wang, H. Study and application of in-situ statistical distribution characterization method of inclusions in wheel profile of large-size EMU. *Meta. Anal.* **2021**, *41*, 1–8.
- Yu, H.; Shao, X.; Zhang, J.; Wang, X. Study on the quantitative relationship between total oxygen and non-metallic inclusions in steel by ASPEX scanning electron microscope. *Chin. J. Eng.* **2015**, *37*, 35–44.
- He, X.; Hu, C.; Xu, L.; Wang, M. Effect of total oxygen content on non-metallic inclusions in gear steel. *Chin. J. Eng.* **2021**, *43*, 537–544.
- Fang, Z.; Sun, Y.; Zhang, X.; Wang, C. Formation and modification of magnesia alumina spinel in oil casing steel. *Iron Steel Vanadium Titan.* **2014**, *35*, 136–141.
- Ji, S.; Zhang, L.; Luo, Y.; Wang, W.; Wang, X. Effect of calcium treatment on non-metallic inclusions in 20CrMnTiH gear steel. *Chin. J. Eng.* **2021**, *43*, 825–834.
- Wang, X.; Li, X.; Li, Q.; Huang, F.; Li, H. Control of string CaO-Al<sub>2</sub>O<sub>3</sub> non-metallic inclusions in X80 pipeline steel plate. *Acta Metall. Sin.* **2013**, *49*, 553–561. [[CrossRef](#)]
- Wang, F. *Reoxidation Phenomenon and Inhibition Mechanism of Aluminum-Deoxidized Steel in Tangsteel*; University of Science and Technology Beijing: Beijing, China, 2019.
- Amezhnov, A.; Rodionova, I. Effect of Non-Metallic Inclusion Chemical and Phase Composition on Corrosion Resistance of Carbon and Low Alloy Steels in Water Media Typical for Oilfield Pipeline Operating Conditions. *Metallurgist* **2019**, *63*, 717–726. [[CrossRef](#)]
- Hou, Z.; Jiang, M.; Yang, E.; Gao, S.; Wang, X. Inclusion characterization in aluminum-deoxidized special steel with certain sulfur content under combined influences of slag refining, calcium treatment, and reoxidation. *Metall. Mater. Trans. B* **2018**, *49B*, 3056–3066. [[CrossRef](#)]
- Murakami, Y.; Endo, M. Effects of defects, inclusions and inhomogeneities on fatigue strength. *Int. J. Fatigue* **1994**, *16*, 163–182. [[CrossRef](#)]
- Li, S.; Zeng, Y.; Tong, K. Micro behavior of inclusions in X80 pipeline steel under fatigue load. *Acta Petrol.* **2012**, *33*, 506–512.
- Ito, Y.; Masumitsu, N.; Matsubara, K. Formation of manganese sulfide in steel. *ISIJ Int.* **1981**, *21*, 477–484. [[CrossRef](#)]
- Takada, H.; Bessho, I.; Ito, I. Effect of sulfur content and solidification variables on morphology and distribution of sulfide in steel ingots. *ISIJ Int.* **2019**, *18*, 564–573. [[CrossRef](#)]
- He, X.; Xu, L.; Wang, M.; Wang, Z. Effect of calcium and magnesium treatment on sulfide inclusions in 38MnVS steel. *Heat Treat. Met.* **2019**, *44*, 90–95.

31. Ruan, Q.; Qian, G.; Pan, J.; Chen, X.; Cheng, G. Effect of titanium containing stainless steel inclusions on submerged nozzle blockage. *Steelmak* **2016**, *32*, 39–43.
32. Zhang, H.; Cheng, W.; Wu, D.; Zheng, H. Study on nodulation mechanism of submerged nozzle for continuous casting of titanium bearing ferritic stainless steel. *Iron Steel Vanadium Titan.* **2010**, *31*, 63–66. [[CrossRef](#)]
33. Zhang, H.; Chen, W.; Zheng, H. Study on the control of titanium oxide inclusions in titanium bearing ferritic stainless steel. *ShangHai Met.* **2010**, *32*, 20–23.

**Disclaimer/Publisher’s Note:** The statements, opinions and data contained in all publications are solely those of the individual author(s) and contributor(s) and not of MDPI and/or the editor(s). MDPI and/or the editor(s) disclaim responsibility for any injury to people or property resulting from any ideas, methods, instructions or products referred to in the content.